Journal of Materials Chemistry A

PAPER

Cite this: J. Mater. Chem. A, 2016, 4, 19045

Catalyzed $KSiH_3$ as a reversible hydrogen storage material†

R. Janot,*[a] W. S. Tang,[bc] D. Clémençon[a] and J.-N. Chotard[a]

Received 1st September 2016
Accepted 9th November 2016

DOI: 10.1039/c6ta07563k

www.rsc.org/MaterialsA

Solid-state hydrogen storage through the reversible formation of metallic hydrides is a key issue for the development of hydrogen as an energy vector. Herein we report the hydrogen storage performances of the $KSiH_3$ phase ball-milled with NbF_5 as a catalyst. The kinetics of hydrogen absorption/desorption are strongly enhanced by the addition of a catalyst as revealed by the large decrease of activation energies for both the absorption and desorption reactions. No disproportionation phenomenon is observed, indicating that the reaction between $KSiH_3$ and KSi is perfectly reversible with a hydrogen storage capacity of 4.1 wt% H_2. The thermodynamic properties of this KSi/$KSiH_3$ equilibrium were investigated by plotting PCI curves from 90 °C to 130 °C: an enthalpy of 24.3 kJ mol^{-1} H_2 and a low entropy change of 59.5 J K^{-1} mol^{-1} H_2 are found. This low entropy variation is related to the high mobility of the H atoms in the α-$KSiH_3$ phase as recently demonstrated by Quasi-Elastic Neutron Scattering (QENS) experiments.

Introduction

In recent years, there has been an increasing interest in the study of different hydrogen storage compounds, particularly for complex hydrides because of their high theoretical gravimetric capacities.[1–3] Various materials comprising light weight elements, like amides $M(NH_2)_x$/imides $M(NH)_{x/2}$,[4–12] alanates $M(AlH_4)_x$ or $M_x(AlH_6)_y$,[13–21] borohydrides $M(BH_4)_x$,[22–32] are some examples that have been well investigated. A recent review on the hydrogen storage properties of the different families of complex hydrides was recently published.[3]

Looking back in the literature, another notable class of hydrides is the alkali silanide $MSiH_3$ family. $KSiH_3$ was the first alkali silanide synthesized by Ring *et al.* in 1961 through a wet chemistry method:[33] excess potassium was mixed with silane gas (SiH_4) in monoglyme at −78 °C. Subsequently in 1968, the potassium to cesium analogues were successfully synthesized by Amberger *et al.*[34] using a similar wet chemistry method of mixing the alkali metal with SiH_4 in monoglyme/diglyme at 20 °C. All three silanides crystallize in the same cubic $Fm\bar{3}m$ space group with cell parameter values of a = 7.23(1), 7.52(1), and 7.86(1) Å for $KSiH_3$, $RbSiH_3$, and $CsSiH_3$, respectively.[35] Finally in 1989, during differential thermal analysis performed on $KSiH_3$, Mundt *et al.* observed a reversible phase transition between the high-temperature cubic α-phase and a low-temperature β-phase.[36] X-ray diffraction performed at −110 °C confirmed a different phase at low temperature: β-$KSiH_3$ crystallizes in the *Pnma* orthorhombic space group with no apparent disorder, consisting of isolated potassium cations and the pyramidal silanide $[SiH_3]^-$ anionic group. A short silicon–hydrogen bond distance of 1.44 Å was found, comparable to the value in gaseous SiH_4 (d_{Si-H} = 1.40 Å). The $MSiH_3$ silanides can be therefore considered as complex hydrides with a SiH_3^- covalent group, similar to AlH_4^- in $MAlH_4$ alanates and BH_4^- in MBH_4 borohydrides.

Recently, we have reported the hydrogenation properties of the MSi Zintl phases.[37–40] Zintl phases possess chemical properties in between the intermetallic and ionic compounds with extended polyanions matching the Zintl–Klemm concept, *i.e.* the polyanion structure is similar to a neighbouring isoelectronic element.[41–43] The heavier alkali congeners (MSi, M = Na, K, Rb, Cs) contain isolated $[Si_4]^{4-}$ tetrahedra (isoelectronic with white phosphorus P_4): NaSi is found in the $C2/c$ monoclinic unit cell[44] and the others in cubic $P\bar{4}3n$ ones.[45] These alkali silicides are extremely air and moisture sensitive. On the other hand, LiSi does not possess the same Zintl phase structure and crystallizes in the $I4_1/a$ tetragonal unit cell with a three-dimensional silicon network (analogous to black phosphorus).[46,47] This LiSi phase is usually obtained by high temperature and pressure synthesis methods (600 °C, 4 GPa),[48] but we have since demonstrated that it can be alternatively obtained by a much more convenient method *i.e.* simple ball-milling of elemental Li and Si under argon.[39]

[a]Laboratoire de Réactivité et Chimie des Solides (LRCS), UMR 7314 CNRS, Université de Picardie Jules Verne, 33 rue Saint-Leu, 80039 Amiens Cedex, France. E-mail: raphael.janot@u-picardie.fr; Fax: +33 3 22 82 75 90; Tel: +33 3 22 82 79 01

[b]NIST Center for Neutron Research, National Institute of Standards and Technology, Gaithersburg, MD 20899-6102, USA

[c]Department of Materials Science and Engineering, University of Maryland, College Park, MD 20742-2115, USA

† Electronic supplementary information (ESI) available: Fig. S1. SEM micrograph of NbF_5 ball-milled for 6 hours. Fig. S2. XRD diagrams of (a) the as-prepared KSi, (b) KSi milled with 5 wt% NbF_5 for one hour, (c) hydrogenated KSi and (d) hydrogenated NbF_5-catalyzed KSi. See DOI: 10.1039/c6ta07563k

The hydrogenation of the monosilicide MSi Zintl phases with heavy alkali metals (M = K, Rb, Cs) into their corresponding silanide complex hydrides α-$MSiH_3$ shows reversible hydrogen absorption–desorption equilibrium within a good temperature-pressure window.[40] In all three systems, pristine MSi absorbs 3 H/fu to form α-$KSiH_3$, α-$RbSiH_3$, and α-$CsSiH_3$, with capacities of 4.3, 2.6, and 1.85 wt% H_2, respectively, and the corresponding alloy is re-obtained upon desorption. The systems undergo huge volume expansion upon hydrogenation, with the CsSi/α-$CsSiH_3$ equilibrium having a value of 56%, the highest ever reported for hydrogenation reactions in the literature.[40] We have also shown an enthalpy–entropy compensation effect for the MSi/α-$MSiH_3$ equilibrium: a concomitant linear increase in the enthalpy (more stable silanide) and entropy change (more localized H atoms in the crystal structure) for the larger cation (Cs^+). Because of this linear thermodynamic increment, a desorption temperature of *ca.* 136 °C at 1 bar hydrogen equilibrium pressure is obtained for all three alkali monosilicide–silanide systems, re-emphasizing their reversibility under near ambient conditions. From this investigation, alkali silanides $M^+[SiH_3]^-$ appear to be an interesting new class of compounds for solid-state hydrogen storage.

From an application point of view, KSi/$KSiH_3$ remains the most interesting due to its higher storage capacity of 4.3 wt% H_2.[37,40] Unfortunately, the kinetics of this system are quite slow for the as-prepared KSi powder, taking several hours for complete absorption at 100 °C and complete desorption at 200 °C.[37] In our previous study, the absorption kinetics were strongly enhanced by ball-milling KSi with 10 wt% carbon black with the initial rate of absorption increased by an order of magnitude. However, without proper control of the exothermicity during hydrogenation, we were otherwise confronted with a disproportionation phenomenon,[38] *i.e.* the formation of KH and the K_8Si_{46} clathrate phase instead of $KSiH_3$. Definitively, for fast hydrogenation, good heat management is required to make the KSi/α-$KSiH_3$ system fully reversible. More recently, a Japanese group has shown that mesoporous Nb_2O_5 is a very effective catalyst for enhancing the hydrogen release kinetics of $KSiH_3$.[49] By ball-milling KSi with 5 mol% (16 wt%) Nb_2O_5, the $KSiH_3$ desorption activation energy decreased from 142 kJ mol^{-1} for the pristine material to 63 kJ mol^{-1} for the catalyzed sample. In addition, the same group also discussed the disproportionation issue during fast hydrogenation, under similar conditions but with different steps: one KSi sample was hydrogenated by first introducing hydrogen pressure at room temperature and then increasing the temperature to 100 °C; whereas another KSi sample was hydrogenated by first heating to 100 °C under vacuum and then an instant exposure to 50 bar H_2. The latter disproportionates into unfavourable products of KH and Si due to the sudden drastic exothermic thermal release, while the sole $KSiH_3$ product following the first pathway maintains the reversible characteristic of the KSi/$KSiH_3$ transformation.[49]

In this paper, we investigate the effects of NbF_5 addition on the absorption/desorption kinetics of the KSi/α-$KSiH_3$ system. The thermodynamics of the KSi/α-$KSiH_3$ equilibrium are also finely reinvestigated thanks to PCI (Pressure–Composition–Isotherm) curves obtained by thermogravimetry on the NbF_5-catalyzed $KSiH_3$ material.

Experimental

As the KSi powders are extremely air and moisture sensitive, they were carefully handled in an argon-filled glovebox (O_2 and H_2O levels below 10 ppm).

Synthesis

KSi alloys were synthesized by solid-state reactions between elemental alkali metal (potassium cubes 5 × 5 × 5 mm) and silicon powder (<40 μm) with a slight excess of silicon (3 mol%) into stainless steel sealed tubes. A silicon excess was used to avoid any traces of unreacted metallic K and thus to avoid any traces of KH after hydrogenation, which would be harmful for the precise determination of the hydrogen absorption/desorption properties of the KSi compound. The tubes were sealed by arc-welding in the glovebox and then placed in a resistance furnace. The samples were annealed at 500 °C for 3 days using a heating rate of 1 °C min^{-1} and then cooled down to room temperature for *ca.* 6 hours.

Commercial NbF_5 powder (Sigma-Aldrich[50]) was ball-milled with a SPEX 8000 mixer-mill using a 50 cc hardened steel milling jar and 10 mm steel balls. The balls-to-powder weight ratio was 40. After 6 hours of milling, the NbF_5 particle size was typically in the 200–500 nm range as observed from scanning electron microscopy (*cf.* Fig. S1 in the ESI†). KSi was then ball-milled under argon with 5 wt% of this premilled NbF_5 using a Retsch PM100 planetary miller. As above, a 50 cc hardened steel milling jar and 10 mm milling balls were used and the balls-to-powder weight ratio was 40.

Structure

X-ray powder diffraction (XRPD) was performed using a Bruker D8 Advanced diffractometer with Cu radiation ($\lambda_1 = 1.54056$ Å, $\lambda_2 = 1.54439$ Å) equipped with a LynxEye detector. Airtight X-ray sample holders with Be windows were used for keeping the samples out of air and moisture. To obtain the composition of the samples (*e.g.* the amount of the different phases), XRPD data were refined using the Fullprof software.

Morphology

Scanning Electron Microscopy (SEM) was performed using a FEI Quanta 200F microscope equipped with an Oxford EDX spectrometer. Sample powders were deposited onto carbon stickers in the glovebox and then introduced into the microscope through the use of a specifically developed transfer chamber. EDX spectroscopy was used to check the K to Si ratio of the KSi phases and to get a chemical mapping of the dispersion of Nb throughout the samples after milling.

Thermal analysis

Differential Scanning Calorimetry (DSC) measurements were carried out under an argon flow by using a Netzsch DSC204

calorimeter. Aluminium crucibles were sealed in the glovebox and put on the DSC calorimeter under argon flow. The cap of the crucible was holed just before the experiment in order to allow gas release upon heating. Different heating rates (1 to 20 °C min^{-1}) were used in order to determine the activation energy of the desorption process using the Kissinger method.

Hydrogenation properties

The absorption/desorption PCI (Pressure-Composition-Isotherm) curves were recorded by the gravimetric method using a Hiden IGA001 gravimetric analyzer. The working pressure of this apparatus can vary from secondary vacuum to 20 bar of hydrogen (Air Liquide Alphagaz 1, a purity of 99.999%). The sample weight was typically of the order of 100 mg and the powder was loaded in a stainless steel bucket in the glovebox. The bucket was hung to the thermobalance under argon using a specially designed transfer chamber. The gravimetric method was used here, instead of the volumetric one, as it allows a precise kinetic analysis under perfectly isobaric conditions (*i.e.* for the volumetric method, the quantity of hydrogen is calculated from pressure changes and therefore the kinetics investigations are not isobaric). The kinetics of the NbF_5-catalyzed KSi powders were determined at 4 different temperatures (90, 110, 130 and 150 °C) with 10 bar of hydrogen for the absorption and 0.1 mbar for desorption.

Results and discussion

After 3 days of annealing at 500 °C, the KSi compound is pure as determined from X-ray diffraction (*cf.* Fig. S2 in the ESI,† XRD diagram labelled (a)), and its particle size is in the 10–100 μm range as observed in the SEM micrograph shown in Fig. 1a. After ball-milling with NbF_5 for one hour, the size is drastically reduced with the larger particles having a 5 μm diameter and most of the particles around 1–2 μm (*cf.* Fig. 1b). Thanks to EDX mapping, it has been checked that the K/Si ratio is very close to one over the whole sample and that Nb is homogeneously dispersed in the ball-milled material. We notice that the surface of the particles remained "clean" without any bubble-like shapes as previously observed for slightly oxidized KSi powders.[38] This highlights that this ball-milled KSi sample is free from oxidation. The XRD diagram obtained on the ball-milled NbF_5-catalyzed sample (*cf.* Fig. S2,† diagram (b)) reveals a strong KSi amorphization with very broad reflections. No other reflection is observed indicating the high dispersion/small particle size of the Nb-containing species. Actually, the amount of added NbF_5 is low in this material (5 wt% *i.e.* 1.8 mol%) and the identification of the exact nature of the Nb-containing species obtained after ball-milling is impossible here by X-ray diffraction. The ball-milling of KSi with NbF_5 leads probably to the formation of KF and Nb or Nb-based compounds with a low Nb oxidation state. As a matter of fact, KSi is a strong reducing agent: this is a Zintl phase consisting of K^+ cations and very reducing $[Si_4]^{4-}$ tetrahedral polyanions. KSi is therefore able to easily reduce Nb^{5+} to lower oxidation states or even metallic niobium. In addition, we have shown in previous studies that potassium can be easily extracted from KSi, either electrochemically,[51] or by ball-milling.[39] In the latter case, for instance, the ball-milling of KSi with LiF leads to the formation of LiSi and KF. Owing to these previous results, it is strongly plausible that the ball-milling of KSi with NbF_5 leads to the formation of KF and Nb or Nb-based compounds, but their existence cannot be demonstrated by X-ray diffraction due to their too low concentrations in the present material. Further experiments, for instance Transmission Electron Microscopy (TEM)/electron diffraction for KF detection and X-ray Photoelectron Spectroscopy (XPS) for Nb oxidation state determination, are needed.

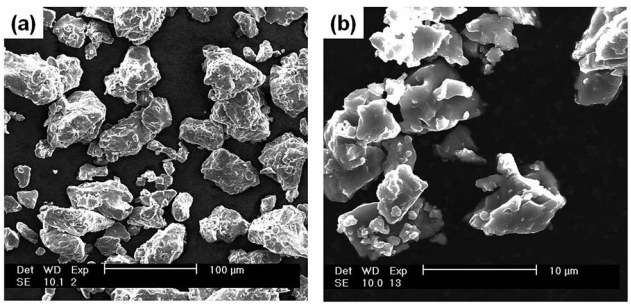

Fig. 1 Scanning Electron Micrographs (SEM) of (a) the as-prepared KSi and (b) KSi milled with 5 wt% NbF_5 for one hour.

There are many reports in the literature about the nature of Nb-based catalysts when used for the MgH_2 kinetics enhancement.[52–54] For sure, Nb^{5+} is reduced upon ball-milling to lower oxidation states (+2 or even the metallic state) and the possible formation of NbH_x hydrides is also reported. The nature of the Nb-containing phase acting as the effective catalyst is still discussed in the hydrogen storage community. About the Japanese report on the use of Nb_2O_5 as a catalyst for $KSiH_3$, XPS experiments showed the formation of NbO after milling and it is assumed that this phase is actually responsible for the kinetics enhancement.[49]

Both pristine KSi and catalyzed KSi were exposed to 10 bar of H_2 and then heated at 150 °C for 10 hours. In both cases, the XRD patterns measured on the hydrogenated powders reveal that all the XRD reflections can be indexed to the $Fm\bar{3}m$ cubic unit cell of the α-$KSiH_3$ polymorph (*cf.* Fig. S2,† diagrams (c and d)). Unreacted KSi is not present and no disproportionation process has occurred upon hydrogenation. The hydrogen release behaviour of these two hydrogenated powders was then investigated by DSC calorimetry as displayed in Fig. 2. A single sharp endothermic peak is observed at 168 °C for the catalyzed-material (at a heating rate of 10 °C min^{-1}), whereas the hydrogen release occurs above 200 °C for the pristine $KSiH_3$ powder (*cf.* Fig. 2). For non-catalyzed hydrogenated KSi, the hydrogen release actually exhibits two broad endothermic peaks at about 215 and 265 °C, probably due to different particle sizes of $KSiH_3$. Clearly, the NbF_5 addition by ball-milling strongly decreased the hydrogen desorption temperature of $KSiH_3$. It is worth mentioning that, in our case, longer milling time does not lead to a further decrease of the hydrogen release

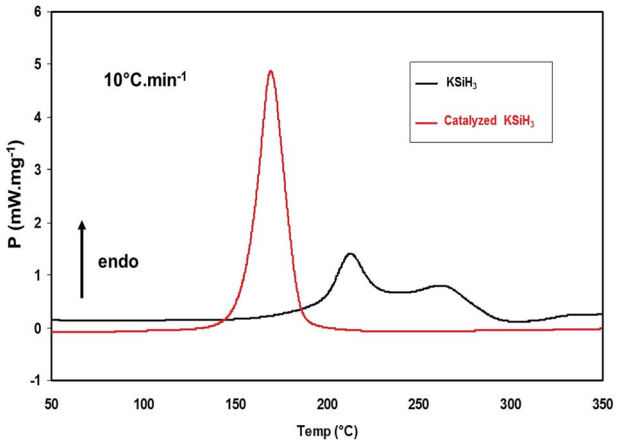

Fig. 2 Differential scanning calorimetry at 10 °C min^{-1} for $KSiH_3$ and NbF_5-catalyzed $KSiH_3$.

temperature as recorded by DSC calorimetry and does not lead to faster hydrogen release kinetics.

Kinetic investigation

In order to determine the activation energy of the hydrogen desorption reaction, DSC calorimetry was performed at different heating rates (2, 5, 10 and 20 °C min^{-1}). As expected, a faster heating rate leads to a higher peak maximum related to the hydrogen release reaction (*cf.* Fig. 3). The activation energy was then calculated using the Kissinger equation:

$$\ln K = -E_a/RT_m + \ln(RK_0/E_a)$$

where $K = \beta/{T_m}^2$, β is the heating rate, T_m is the peak maximum temperature, R is the gas constant and E_a is the activation energy of the desorption process. From the slope of the Kissinger plot (*cf.* inset of Fig. 3), an energy of 66.1 kJ mol^{-1} is obtained for NbF_5-catalyzed $KSiH_3$, which is a value largely below the one previously obtained for non-catalyzed $KSiH_3$ (121 kJ mol^{-1}) from isothermal experiments (*i.e.* weight loss as a function of time for a given temperature) using the Arrhenius equation.[38] In a previous attempt to decrease the $KSiH_3$ desorption activation energy, KSi was ball-milled with carbon black,[38] but a disproportionation phenomenon was observed upon hydrogenation with the formation of KH and the clathrate K_8Si_{46} phase instead, probably due to a bad management of the heat generated upon hydrogenation. In the present study, there was no disproportionation reaction as only α-$KSiH_3$ was always detected by X-ray diffraction performed on all the hydrogenated powders.

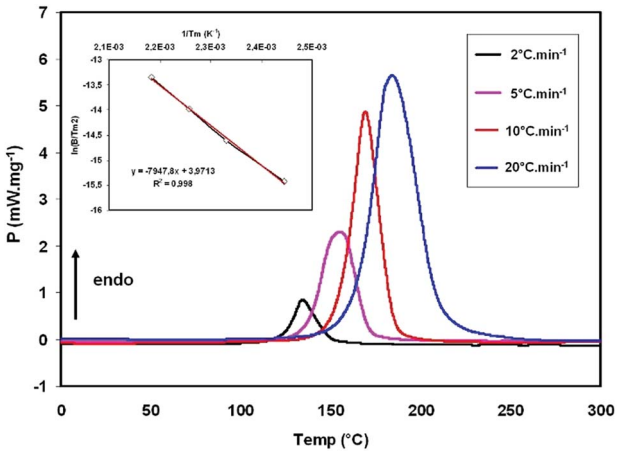

Fig. 3 Differential scanning calorimetry at 4 different heating rates for NbF_5-catalyzed $KSiH_3$. Inset: Kissinger plot allowing the calculation of the activation energy of the desorption reaction.

A Japanese group has investigated the effects of different catalysts such as nano-metals (Ni, Co, Nb), TiO_2, $TiCl_3$ and Nb_2O_5 on the hydrogen release kinetics of $KSiH_3$.[49,55] Although the effect of metal additions appears limited, with the lowest activation energy of 106 kJ mol^{-1} using Ni,[55] a more significant decrease of activation energy was reported with mesoporous Nb_2O_5.[49] A value of 63 kJ mol^{-1} was measured for 20 h-milled KSi with 5 mol% Nb_2O_5 (corresponding to 16 wt% Nb_2O_5), a value similar to the activation energy obtained in our case with only 5 wt% NbF_5. From previous studies made in our laboratory about the effects of catalyst addition on the hydrogen release kinetics of MgH_2,[56,57] the superior effect of NbF_5 compared to Nb_2O_5 was already noticed.[57] This better catalytic effect could be nested in the formation of a $Nb^{\delta+}$–$H^{\delta-}$ bond favoured by the large electronic delocalization of the Nb–F bond (*i.e.* higher electronegativity of F than O in the Nb_xX_5 compound) leading to a further weakening of the surface metal–H bond in the hydride as already discussed in the literature.[57]

In order to confirm the kinetic enhancement observed by DSC, thermogravimetric experiments were performed on the NbF_5-catalyzed KSi sample for both absorption (10 bar H_2) and desorption (0.1 mbar H_2). Fig. 4a shows the curves of hydrogen release at 90, 110, 130 and 150 °C. An experimental hydrogen storage capacity of around 4.1 wt% is measured which is in very good agreement with the theoretical capacity based on the formation of $KSiH_3$ (4.3 wt% hydrogen storage capacity) and the weight of inactive catalyst (5 wt%). The hydrogen release is particularly fast above 130 °C with less than one hour to obtain a complete desorption. The activation energy was calculated using the Arrhenius equation:

$$\ln K = A \exp(-E_a/RT)$$

where K is the reaction rate, R is the gas constant and A is the pre-exponential factor. A value of 61.0 kJ mol^{-1} is obtained (*cf.* inset of Fig. 4a), in good agreement with the energy obtained from the DSC curves and the Kissinger method (66.1 kJ mol^{-1}).

The kinetic investigation upon absorption (10 bar H_2) by the same thermogravimetric method is shown in Fig. 4b. The hydrogenation is fast, taking less than one hour to perform a full absorption at temperatures above 100 °C. The inset of Fig. 4b shows the Arrhenius plot ($\ln K$ as a function of $1/T$) corresponding to the absorption reaction. A low activation energy of 33.2 kJ mol^{-1} is obtained, whereas an energy of 56.0 kJ mol^{-1} was previously determined for pristine KSi.[38] A comparison with the Nb_2O_5-catalyzed KSi material reported in

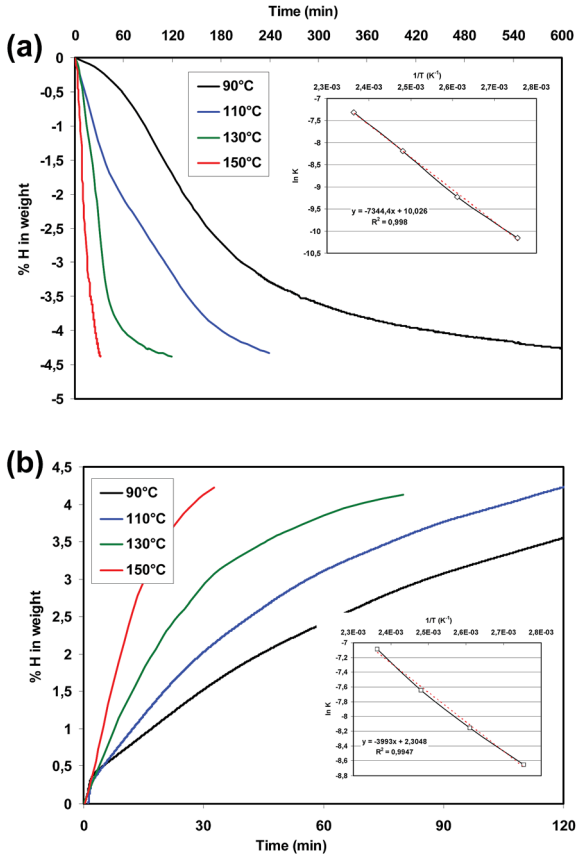

Fig. 4 Kinetics for NbF_5-catalyzed $KSiH_3$ recorded by thermogravimetry at 4 different temperatures. (a) Desorption under 0.1 bar H_2, (b) absorption under 10 bar H_2. Inset: Arrhenius plots allowing the calculation of the activation energies.

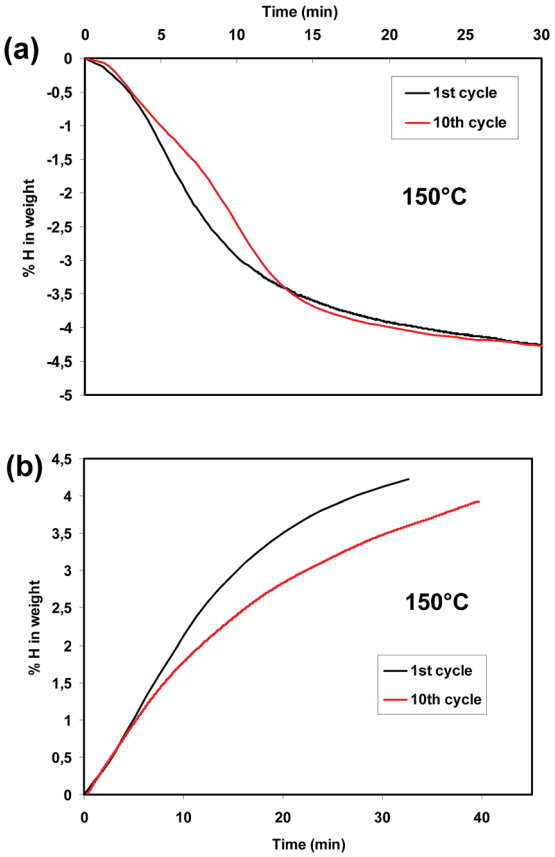

Fig. 5 Kinetics at 150 °C for NbF_5-catalyzed $KSiH_3$ during the 1st and 10th cycles. (a) Desorption under 0.1 bar H_2 and (b) absorption under 10 bar H_2.

the literature[49] is unfortunately not possible since the activation energy upon absorption was not reported for this material.

The cycling stability of the NbF_5-catalyzed KSi sample was then investigated at 150 °C on the same thermogravimetric analyzer (absorption 10 bar H_2 and desorption 0.1 mbar H_2). A very good retention capacity is obtained since the storage capacity still exceeds 4.0 wt% after 10 absorption/desorption cycles as shown in Fig. 5. The shape of the hydrogen release kinetic curve has slightly changed after 10 cycles (*cf.* Fig. 5a), but the overall time needed to perform complete desorption remains the same: around 30 min. For the hydrogen absorption kinetics, a slight decline is noticed after 10 cycles (*cf.* Fig. 5b). It must be noted that a much faster hydrogenation reaction could be attained if the applied hydrogen pressure was increased above 10 bar, since the plateau pressure upon KSi hydrogenation at 150 °C is around 2.6 bar as discussed in the following section.

Thermodynamic investigation

Due to the particularly slow kinetics of the pristine KSi phase, full PCI curves were not plotted in our previous reports on the KSi/α-$KSiH_3$ equilibrium.[37,40] For the determination of the enthalpy and entropy of the absorption/desorption reaction, we have instead measured the equilibrium pressures at the mid-plateau when desorbing $KSiH_3$ at different temperatures. Namely, α-$KSiH_3$ was first desorbed at a certain temperature (T_1) down onto its plateau pressure. To ensure that its corresponding equilibrium pressure was well determined, the value was taken at the mid-plateau of T_1. The sample was then heated up to T_2 and held until the equilibrium pressure was stable, before the temperature was increased to T_3 and so on. In this way, a single PCI was performed on the desorption plateau, with temperature increments only after the equilibrium pressure was well established. At the end of the experiment, the total quantity of hydrogen gas which has been released during the measurement was calculated in order to check whether the measured equilibrium pressure still corresponded to the plateau (two-phase domain) pressure. Using the Van't Hoff equation, enthalpy and entropy values of 22.6 kJ mol^{-1} H_2 and 54.4 J K^{-1} mol^{-1} H_2 were obtained from the $KSiH_3$ desorption, respectively.[40] This very low entropy value was initially surprising, since it was much less than the classical entropy change of around 100–130 J K^{-1} mol^{-1} H_2 usually obtained upon hydrogen desorption of intermetallics[58,59] (*i.e.* the change between the low entropy of H atoms well located in interstitial sites and the large entropy of gaseous H_2 molecules). This low entropy was supported by DFT calculations.[37] Specifically, vibrational analysis and phonon calculations were made by the

direct general approach to lattice dynamics as implemented in the Phonon-MedeA software. By DFT calculations, an enthalpy of 28 kJ mol^{-1} H_2 was found in agreement with the value of 22.6 kJ mol^{-1} H_2 found experimentally. About the entropy change, a value of 62.5 J K^{-1} mol^{-1} H_2 or 52 J K^{-1} mol^{-1} H_2 was found by DFT calculations taking into account the rotational entropy of SiH_3^- or the statistical distribution of H atoms in the 96k Wyckoff positions, respectively. These values correspond well with the entropy change of 54.4 J K^{-1} mol^{-1} H_2 found experimentally for the uncatalyzed-$KSiH_3$ material.

In the paper reporting the excellent catalytic effect of Nb_2O_5 for enhancing the $KSiH_3$ hydrogen release kinetics,[49] a thermodynamic investigation was also performed. Full PCI curves were plotted upon desorption at 150, 175 and 200 °C using a volumetric Sievert apparatus. Significantly different enthalpy and entropy values were obtained: the desorption enthalpy was found to be 40.1 kJ mol^{-1} H_2, while the entropy value was 106 J K^{-1} mol^{-1} H_2. In order to understand this discrepancy between our previous reports and this recent Japanese article, we have also plotted full PCI curves on a catalyzed-$KSiH_3$ sample.

Fig. 6 shows the PCI curves obtained upon absorption and desorption at 150 °C for the NbF_5-catalyzed $KSiH_3$ material and then desorption at 130 °C, 110 °C and 90 °C. For each point observed on the PCI curves, holding durations of 12 hours were used to ensure a perfect equilibrium condition for each pressure step. A significant hysteresis is observed at 150 °C with plateau pressures upon absorption and desorption at about 2.6 and 1.29 bar, respectively. This hysteresis is usually attributed to the extra energy needed for the lattice expansion and resulting mechanical stresses upon hydrogenation. By decreasing the temperature from 150 °C to 90 °C, we observe that the desorption plateau pressure is only slightly shifted from 1.29 bar to 0.41 bar. The corresponding Van't Hoff plot (ln P/P_0 as a function of $1/T$) is shown in the inset of Fig. 6. Using the Van't Hoff equation, enthalpy and entropy values of 24.3 kJ mol^{-1} H_2 and 59.5 J K^{-1} mol^{-1} H_2 are obtained, respectively. These values are in good agreement with those we have previously reported for a non-catalyzed $KSiH_3$ sample, either from experimental measurements, or from DFT calculations, as explained above.[37,40]

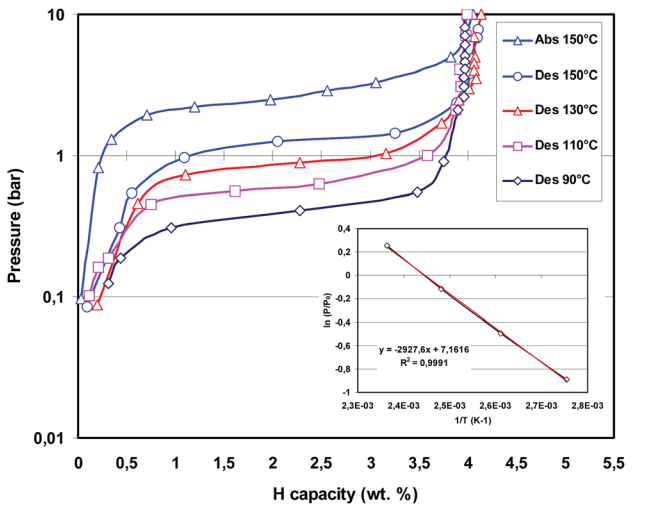

Fig. 6 Pressure-Composition-Isotherms (PCI) curves plotted upon absorption at 150 °C and desorption at 150, 130, 110, and 90 °C for NbF_5-catalyzed $KSiH_3$. Inset: Van't Hoff plot allowing the calculations of the enthalpy and entropy of the desorption reaction.

Recent evidence for the high disorder in the α-$KSiH_3$ silanide comes from neutron scattering experiments. Initially, when neutron powder diffraction (NPD) was performed on the α-$MSiD_3$ compounds (M = K, Rb, Cs), the best refinements were obtained with the deuterium atoms in the 96k Wyckoff site with a low occupancy of 12%, but large thermal factors reflected significant movements within the cubic unit cell.[37,40] However, the nature of the orientational disorder, static or dynamic, was still not yet fully understood. Subsequent strong evidence from spectroscopic analysis suggested that the disorder was dynamic.[60] A Quasi-Elastic Neutron Scattering (QENS) study of α-$KSiH_3$ has confirmed this dynamic disorder.[61] The QENS results show that the order–disorder (β–α) phase transition leads to dynamical changes associated with rapid reorientational motions of the pyramidal SiH_3^- anions.

A study of the dynamical trends in the alkali metal silanides series (with K, Rb, and Cs but also the mixed $M_{0.5}M'_{0.5}SiH_3$ phases) was recently conducted by neutron scattering methods.[62] Interestingly, the reorientational mobility of SiH_3^- decreased when increasing the cation size: α-CsH_3 is more ordered than α-$RbCsH_3$, which in turn is more ordered than α-$KSiH_3$. This experimental observation is in perfect agreement with the enthalpy/entropy compensation effect reported previously.[40] A simultaneous linear increase in the enthalpy (more stable silanide) and entropy change (more localized H atoms in the crystal structure) with increasing cation size was determined from equilibrium pressure measurements. Clearly, the pronounced SiH_3^- dynamics is the reason for the high entropy observed in the disordered α-$KSiH_3$ phase. This leads to the low entropy variation for hydrogen absorption/desorption, which is the main cause of the favourable hydrogen storage properties of these materials.

Conclusions

We have investigated the effects of NbF_5 as a catalyst for enhancing the hydrogen absorption/desorption kinetics of the KSi/$KSiH_3$ system. Through a ball-milling process with NbF_5, the hydrogen release kinetics of α-$KSiH_3$ are strongly enhanced with a complete desorption in less than one hour at temperatures above 130 °C. The activation energy of the desorption reaction is decreased from 121 kJ mol^{-1} for the non-catalyzed material to 61–66 kJ mol^{-1} for the 1 hour NbF_5-milled KSi powder. The catalyzed material exhibits a 4.1 wt% experimental hydrogen storage capacity with a nice retention of its fast kinetics upon cycling. The thermodynamics of the KSi/α-$KSiH_3$ equilibrium were also reinvestigated by plotting PCI curves using a gravimetric analyzer. Enthalpy and entropy values of 24.3 kJ mol^{-1} H_2 and 59.5 J K^{-1} mol^{-1} H_2 were obtained, respectively, confirming our previous reports. In this study, we have therefore been able to strongly promote the hydrogen storage kinetics of the KSi/α-$KSiH_3$ system and to keep

a perfectly reversible reaction near ambient conditions, without any disproportionation phenomenon.

Acknowledgements

The European community and the FEDER program (Fonds Européen de Développement Regional) are gratefully acknowledged for the Ph.D. funding of W. S. Tang. The authors wish to thank Matthieu Courty from LRCS for the DSC experiments.

References

1 L. Schlapbach and A. Züttel, *Nature*, 2001, **414**, 353–358.
2 U. Eberle, M. Felderhoff and F. Schüth, *Angew. Chem., Int. Ed.*, 2009, **121**, 6732–6757.
3 Q. Lai, *et al.*, *ChemSusChem*, 2015, **8**, 2789–2825.
4 P. Chen, Z. Xiong, J. Luo, J. Lin and K. L. Tan, *Nature*, 2002, **420**, 302–304.
5 P. Chen, Z. Xiong, J. Luo, J. Lin and K. L. Tan, *J. Phys. Chem. B*, 2003, **107**, 10967–10970.
6 W. Luo and S. Sickafoose, *J. Alloys Compd.*, 2006, **407**, 274–281.
7 R. Janot, J. B. Eymery and J. M. Tarascon, *J. Power Sources*, 2007, **164**, 496–502.
8 R. Janot, J. B. Eymery and J. M. Tarascon, *J. Phys. Chem. C*, 2007, **111**, 2335–2340.
9 D. H. Gregory, *J. Mater. Chem.*, 2008, **18**, 2321–2330.
10 J. Hu and M. Fichtner, *Chem. Mater.*, 2009, **21**, 3485–3490.
11 J.-B. Eymery, L. Truflandier, T. Charpentier, J.-N. Chotard, J.-M. Tarascon and R. Janot, *J. Alloys Compd.*, 2010, **503**, 194–203.
12 J. Wang, G. Wu, Y. S. Chua, J. Guo, Z. Xiong, Y. Zhang, M. Gao, H. Pan and P. Chen, *ChemSusChem*, 2011, **4**, 1622–1628.
13 B. Bogdanovic and M. Schwickardi, *J. Alloys Compd.*, 1997, **253–254**, 1–9.
14 B. Bogdanovic, R. A. Brand, A. Marjanovic, M. Schwickardi and J. Tolle, *J. Alloys Compd.*, 2000, **302**, 36–58.
15 M. Fichtner, O. Fuhr and O. Kircher, *J. Alloys Compd.*, 2003, **356**, 418–422.
16 M. Mamatha, B. Bogdanovic, M. Felderhoff, A. Pommerin, W. Schmidt, F. Schüth and C. Weidenthaler, *J. Alloys Compd.*, 2006, **407**, 78–86.
17 Y. Kim, E.-K. Lee, J.-H. Shim, Y. W. Cho and K. B. Yoon, *J. Alloys Compd.*, 2006, **422**, 283–287.
18 C. Wolverton and V. Ozolins, *Phys. Rev. B: Condens. Matter Mater. Phys.*, 2007, **75**, 064101.
19 A. Klaveness, P. Vajeeston, P. Ravindran, H. Fjellvag and A. Kjekshus, *J. Alloys Compd.*, 2007, **433**, 225–232.
20 R. D. Stephens, A. F. Gross, S. L. Van Atta, J. J. Vajo and F. E. Pinkerton, *Nanotechnology*, 2009, **20**, 204018.
21 T. K. Nielsen, M. Polanski, D. Zasada, P. Javadian, F. Besenbacher, J. Bystrzycki, J. Skibsted and T. R. Jensen, *ACS Nano*, 2011, **5**, 4056–4064.
22 A. Züttel, S. Rentsch, P. Fischer, P. Wenger, P. Sudan, P. Mauron and C. Emmenegger, *J. Alloys Compd.*, 2003, **356–357**, 515–520.
23 A. Züttel, A. Borgschulte and S. Orimo, *Scr. Mater.*, 2007, **56**, 823–828.
24 P. Mauron, F. Buchter, O. Friedrichs, A. Remhof, M. Bielmann, C. N. Zwicky and A. Züttel, *J. Phys. Chem. B*, 2008, **112**, 906–910.
25 T. Matsunaga, F. Buchter, P. Mauron, M. Bielman, Y. Nakamori, S. Orimo, N. Ohba, K. Miwa, S. Towata and A. Zuìttel, *J. Alloys Compd.*, 2008, **459**, 583–588.
26 S. Cahen, J. B. Eymery, R. Janot and J. M. Tarascon, *J. Power Sources*, 2009, **189**, 902–908.
27 R. Cerny, D. B. Ravnsbæk, G. Severa, Y. Filinchuk, V. D'Anna, H. Hagemann, D. Haase, J. Skibsted, C. M. Jensen and T. R. Jensen, *J. Phys. Chem. C*, 2010, **114**, 19540–19549.
28 P. Schouwink, V. D'Anna, M. B. Ley, L. V. M. Lawson Daku, B. Richter, T. R. Jensen, H. Hagemann and R. Cerny, *J. Phys. Chem. C*, 2012, **116**, 10829–10840.
29 M. B. Ley, D. Ravnsbæk, Y. Filinchuk, Y.-S. Lee, R. Janot, Y. W. Cho, J. Skibsted and T. R. Jensen, *Chem. Mater.*, 2012, **24**, 1654–1663.
30 M. B. Ley, S. Boulineau, R. Janot, Y. Filinchuk and T. R. Jensen, *J. Phys. Chem. C*, 2012, **116**, 21267–21276.
31 I. Dovgaliuk, V. Ban, Y. Sadikin, R. Cerny, L. Aranda, N. Casati, M. Devillers and Y. Filinchuk, *J. Phys. Chem. C*, 2014, **118**, 145–153.
32 M. Depardieu, R. Janot, C. Sanchez, H. Deleuze, C. Gervais, M. Birot, M. Morcrette and R. Backov, *J. Mater. Chem. A*, 2014, **2**, 7694–7701.
33 M. A. Ring and D. M. Ritter, *J. Phys. Chem.*, 1961, **65**, 182–183.
34 E. Amberger, R. Römer and A. Layer, *J. Organomet. Chem.*, 1968, **12**, 417–423.
35 E. Weiss, G. Hencken and H. Kühr, *Chem. Ber.*, 1970, **103**, 2868–2872.
36 O. Mundt, G. Becker, H.-M. Hartmann and W. Schwarz, *Z. Anorg. Allg. Chem.*, 1989, **572**, 75–88.
37 J.-N. Chotard, W. S. Tang, P. Raybaud and R. Janot, *Chem.–Eur. J.*, 2011, **17**, 12302–12309.
38 W. S. Tang, J.-N. Chotard, P. Raybaud and R. Janot, *Phys. Chem. Chem. Phys.*, 2012, **14**, 13319–13324.
39 W. S. Tang, J.-N. Chotard and R. Janot, *J. Electrochem. Soc.*, 2013, **160**, A1232–A1240.
40 W. S. Tang, J.-N. Chotard, P. Raybaud and R. Janot, *J. Phys. Chem. C*, 2014, **118**, 3409–3419.
41 G. J. Miller, in *Chemistry, Structure and Bonding of Zintl Phases and Ions*, ed. S. M. Kauzlarich, VCH, New York, 1996, p. 1.
42 R. Nesper, *Angew. Chem., Int. Ed.*, 1991, **30**, 789–817.
43 J. D. Corbett, *Chem. Rev.*, 1985, **85**, 383–397.
44 T. Goebel, Y. Prots and F. Haarmann, *Z. Kristallogr.–New Cryst. Struct.*, 2008, **223**, 187–188.
45 H. G. von Schnering, M. Schwarz, J.-H. Chang, K. Peters, E. M. Peters and R. Nesper, *Z. Kristallogr.–New Cryst. Struct.*, 2005, **220**, 525–527.
46 J. Evers, G. Oehlinger and G. Sextl, *Angew. Chem., Int. Ed.*, 1993, **32**, 1442–1444.
47 J. Evers, G. Oehlinger and G. Sextl, *Eur. J. Solid State Inorg. Chem.*, 1997, **34**, 773–784.

48 L. A. Stearns, J. Gryko, J. Diefenbacher, G. K. Ramachandran and P. F. McMillan, *J. Solid State Chem.*, 2003, **173**, 251–258.
49 A. Jain, T. Ichikawa, S. Yamaguchi, H. Miyaoka and Y. Kojima, *Phys. Chem. Chem. Phys.*, 2014, **16**, 26163–26167.
50 The mention of all commercial suppliers in this paper is for clarity. This does not imply the recommendation or endorsement of these suppliers by NIST.
51 V. Seznec, P. Senguttuvan, D. Larcher and J.-M. Tarascon, *ECS Electrochem. Lett.*, 2015, **4**(10), A119–A123.
52 G. Barkhordarian, T. Klassen and R. Bormann, *Scr. Mater.*, 2003, **49**, 213–217.
53 G. Barkhordarian, T. Klassen and R. Bormann, *J. Alloys Compd.*, 2004, **364**, 242–246.
54 O. Friedrichs, F. Aguey-Zinsou, J. R. Ares Fernandez, J. C. Sanchez-Lopez, A. Justo, T. Klassen, R. Bormann and A. Fernandez, *Acta Mater.*, 2006, **54**, 105–110.
55 A. Jain, H. Miyaoka, T. Ichikawa and Y. Kojima, *J. Alloys Compd.*, 2015, **645**, S144–S147.
56 V. Bhat, A. Rougier, L. Aymard, X. Darok, G. Nazri and J.-M. Tarascon, *J. Power Sources*, 2006, **159**, 107–110.
57 N. Recham, V. Bhat, M. Kandavel, L. Aymard, J.-M. Tarascon and A. Rougier, *J. Alloys Compd.*, 2008, **464**, 377–382.
58 A. Züttel, *Naturwissenschaften*, 2004, **91**, 157–172.
59 S. V. Alapati, J. K. Johnson and D. S. Sholl, *Phys. Chem. Chem. Phys.*, 2007, **9**, 1438–1452.
60 V. F. Kranak, Y. C. Lin, M. Karlsson, J. Mink, S. T. Norberg and U. Haussermann, *Inorg. Chem.*, 2015, **54**, 2300–2309.
61 C. Osterberg, H. Fahlquist, U. Haussermann, C. M. Brown, T. J. Udovic and M. Karlsson, *J. Phys. Chem. C*, 2016, **120**, 6369–6376.
62 W. S. Tang, M. Dimitrievska, J.-N. Chotard, W. Zhou, R. Janot, A. Skripov and T. J. Udovic, *J. Phys. Chem. C*, 2016, **120**, 21218–21227.